Journal of
Materials Chemistry A

Materials for energy and sustainability

Accepted Manuscript

This article can be cited before page numbers have been issued, to do this please use: X. Wang, B. Wang, Y. Tang, B. Xu, C. Liang, M. Yan and Y. Jiang, *J. Mater. Chem. A*, 2020, DOI: 10.1039/C9TA12376H.

ROYAL SOCIETY OF CHEMISTRY

rsc.li/materials-a

View Article Online
DOI: 10.1039/C9TA12376H

ARTICLE

Manganese hexacyanoferrate reinforced by PEDOT coating toward high-rate and long-life sodium-ion battery cathode

Received 00th January 20xx,
Accepted 00th January 20xx

DOI: 10.1039/x0xx00000x

Xiao Wang,[a] Baoqi Wang, [a] Yuxin Tang,[b] Ben Bin Xu,[c] Chu Liang,[d] Mi Yan,[a] Yinzhu Jiang[a*]

Prussian blue analogues hold great promise as cathodes in sodium ion batteries. Among Prussian blue analogues, manganese hexacyanoferrate is desirable because of its high working voltage, as well as its high specific capacity and low cost. However, poor cycling stability and unsatisfied rate capability of manganese hexacyanoferrate, which are mainly caused by poor intrinsic conductivity, phase transition, side reactions and transition metal dissolution, extremely limits its practical application. In this work, we demonstrate a high-rate and long-life MnHCF@PEDOT sodium ion battery cathode through a facile in-situ polymerization method. Benefitting from the synergistic effect of the inhibited Mn/Fe dissolution, suppressed phase transition and improved capacitive storage, the composite electrode exhibits a high capacity of 147.9 mAh g^{-1} at 0.1 C, 95.2 mAh g^{-1} at a high rate of 10 C and 78.2% capacity retention after 1000 cycles. Furthermore, even at a low temperature of -10 °C, MnHCF@PEDOT still delivers a high capacity of 87.0 mAh g^{-1} and remains 71.5 mAh g^{-1} (82.2 %) after 500 cycles.

Introduction

Advanced large-scale energy storage system (ESS) is much desirable to meet the rapid development of clean and sustainable energies such as solar and wind due to their instability and intermittence.[1-4] Sodium-ion batteries (SIBs) are amongst the most attractive energy storage techniques due to the abundant and low-cost sodium resources, as well as their similar working principle to lithium-ion batteries (LIBs).[5-8] Exploring a suitable cathode material is critical for the development of SIBs considering the larger ion radius of sodium and the higher redox potential of Na/Na^+ as compared to those of lithium.[9-11] Prussian blue and its analogues (PBAs) have attracted extensive attention as cathode materials for SIBs because of their ease of synthesis, open framework structure and high theoretical capacity (~170 mAh g^{-1}).[12-20]

Among the PBAs, manganese hexacyanoferrate (MnHCF) exhibits a high redox potential in high spin Mn^{HS} configuration as compared to other transition metals, which makes MnHCF more competitive in delivering higher output voltage and energy density.[20-23] However, MnHCF as cathode material suffers from poor cycling and high polarization on account of its poor conductivity and side reactions with the electrolyte, as well as the phase transition and dissolution of Mn during cycling.[26-29] A massive efforts have been devoted into improving the electrochemical performance of MnHCF, such as hetero transition metal doping,[30, 31] removal of interstitial H_2O,[32] and conductive polymer/carbon coating.[33, 34] However, realizing a high-rate and long life MnHCF-based cathode is still a tough challenge considering the cooperative Jahn-Teller distortion in structure of Mn(III)-based electrodes.

In this work, we report a facile in-situ polymerization method for the synthesis of MnHCF@PEDOT composite through employing MnHCF cubes as both template and oxidation initiator. The inhibited dissolution of Mn/Fe, suppressed phase transition and improved capacitive storage benefitted from the PEDOT coating greatly promote the sodium storage performance. A high reversible capacity of 147.9 mAh g^{-1} at 0.1 C and an ultra-long cycle life (78.3% capacity retention after 1000 cycles at 10 C) are demonstrated. Furthermore, the composite shows impressive low-temperature performance at -10 °C, delivering a high capacity of 87.7 mAh g^{-1} and a capacity retention of 82.2% after 500 cycles at 1 C.

Experimental

Synthesis of MnHCF and MnHCF@PEDOT

MnHCF was synthesized by a co-precipitation method as described in other literatures with minor modifications.[36, 37] In a typical preparation, 3 mmol $Na_4Fe(CN)_6{\cdot}10H_2O$, 0.24 mol NaCl, and 12 mmol sodium citrate were dissolved in 100 mL deionized(DI) water with magnetic stirring to form solution A. 6 mmol $MnSO_4{\cdot}4H_2O$ was dissolved in 100 mL DI water with magnetic stirring to form solution B. Solution B was added into solution A (90 °C) by a peristaltic pump at a rate of 1 mL min^{-1} under magnetic stirring condition and N_2 atmosphere. The white suspension was aged for 3 h under continuous stirring at 90 °C after solution B was used up. The obtained white precipitate was collected by centrifugation and

[a] State Key Laboratory of Silicon Materials, Key Laboratory of Novel Materials for Information Technology of Zhejiang Province and School of Materials Science and Engineering, Zhejiang University, Hangzhou 310027, P. R. China. E-mail: yzjiang@zju.edu.cn
[b] Institute of Applied Physics and Materials Engineering, University of Macau, Macau 999078, P. R. China.
[c] Smart Materials and Surfaces Lab, Mechanical Engineering, Faculty of Engineering and Environment, Northumbria University, Newcastle upon Tyne NE1 8ST, U.K.
[d] College of Materials Science and Engineering, Zhejiang University of Technology, Hangzhou 310014, P. R. China

Electronic Supplementary Information (ESI) available: Additional TG, XPS, SEM, galvanostatic charge–discharge profile, XRD and CV test. See DOI: 10.1039/x0xx00000x

washed by DI water and ethanol thoroughly before dried in vacuum at 110 °C for 24 h.

A certain amount of 3, 4-ethylenedioxythiophene (EDOT) was dispersed in 40 mL DI water and then stirred for 0.5 h. Meanwhile, 200 mg as-synthesized MnHCF and 100 mg $(NH_4)_2S_2O_8$ were dispersed in 10 mL DI water by magnetic stirring and ultrasonication. Then, MnHCF/ $(NH_4)_2S_2O_8$ suspension was added into EDOT suspension immediately, followed by 10-hour magnetic stirring at room temperature. The obtained greyish-green precipitate was collected by centrifugation and washed by DI water and ethanol thoroughly before dried in vacuum at 80 °C for 24 h. The as-synthesized powder was named MnHCF@PEDOT-10, MnHCF@PEDOT-20, and MnHCF@PEDOT-50 according to the amount of EDOT (10, 20 and 50 µL, respectively). As a comparison, bare PEDOT was prepared by the same method without the addition of MnHCF.

Materials characterization

The X-ray diffraction (XRD) patterns were acquired on Bruker D8 Advance X-ray diffractometer with Co K_α radiation (λ=0.178897nm) at a scan rate of 2 º min^{-1}. The samples for ex-situ XRD were prepared in the coin cells during the 11th cycle at 1 C. The molar ratios of Na, Mn and Fe were measured by inductively coupled plasma-optical emission spectrometry (ICP-OES, Optima 8000), and the contents of C, H and N were analyzed by elemental analysis (EA, Vario Micro). Raman spectra were collected by LabRAM HR Evolution Raman spectrometer under an Ar ion laser with a wavelength of 532 nm. The X-ray photoelectron spectra (XPS) were recorded on Thermo Scientific K-Alpha+ X-ray photoelectron spectrometer. Thermogravimetric (TG) analyses were carried out on TA-Q500 from 50 to 450 °C at a heating rate of 5 °C min^{-1} in air to determine the water content and the amount of PEDOT in as-synthesized samples. Scanning electron microscopy (SEM, Hitachi S-4800) and transmission electron microscopy (TEM, JEM-2100) were used to characterize the morphologies of all samples.

Electrochemical measurements

The as-synthesized samples, Ketjen black and polyvinylidene fluoride (PVDF) with a mass ratio of 7:2:1 were mixed and dissolved in N-methyl pyrrolidinone (NMP) to make a slurry. The slurry was casted on Al foil and then dried at 80 °C in vacuum for 24 h to prepare working electrodes. The average mass loading of the electrodes was about 2 mg cm^{-2}. CR2025 coin cells using the as-prepared electrodes as cathodes were assembled in an Ar-filled glovebox with H_2O and O_2 contents less than 1 ppm. Metallic sodium, 1 M $NaPF_6$ in ethylene carbonate/diethylene carbonate (EC/DEC, 1:1 in volume) with 5 vol% fluoroethylene carbonate (FEC) as the additive, and Whatman GF/D glass microfiber filters were used as anode, electrolyte and separator, respectively. Galvanostatic charge-discharge test at different current densities were carried out on a Neware battery testing system at 30 °C with a voltage range of 2.0-4.0 V. And the specific capacity is calculated based on the mass of the as-synthesized samples. Cyclic voltammetry (CV) and electrochemical impedance spectroscopy (EIS) were carried out on a CHI604E electrochemical workstation. The voltage range of CV was 2.0-4.0 V and the scan rates ranged from 0.1 to 2 mV s^{-1}. The frequency range of EIS was 10^{-2}-10^5 Hz with an amplitude of 5 mV.

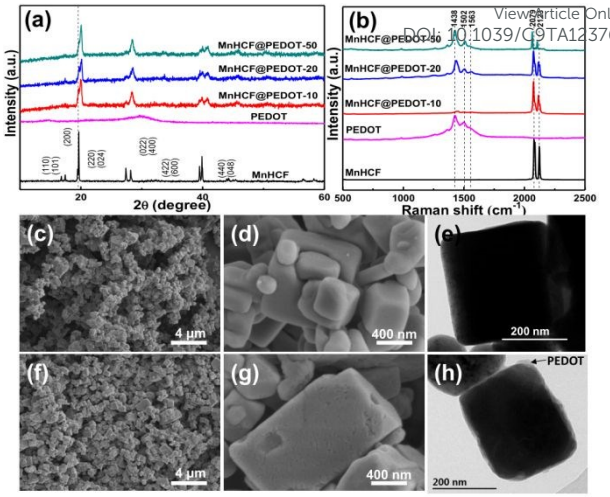

Fig. 1 (a) XRD patterns and (b) Raman spectra of the MnHCF, PEDOT and MnHCF@PEDOT-10/20/50; (c, d) SEM and (e) TEM images of MnHCF; (f, g) SEM and (h) TEM images of MnHCF@PEDOT-20.

Results and discussion

A facile co-precipitation method was carried out for the synthesis of bare MnHCF, which was used as template and oxidation initiator for in-situ polymerization of EDOT to obtain a series of MnHCF@PEDOT-10/20/50 composites varied in the amount of EDOT. **Fig. 1**a shows the X-ray diffraction (XRD) patterns of the bare MnHCF and the MnHCF@PEDOT composites. Due to the lattice distortion caused by the high sodium content, bare MnHCF was crystallized into monoclinic structure rather than a cubic one, which is consistent with the previous reports.[20, 23] The monoclinic phase of MnHCF is remained after PEDOT coating, implying the reserved Na-rich nature. According to the TG profiles (**Fig. S1**), ICP-OES measurement and elemental analyses, the formula of MnHCF can be calculated as $Na_{1.85}Mn[Fe(CN)_6]_{0.98}\square_{0.02}\cdot 2.34H_2O$, while MnHCF@PEDOT-10, MnHCF@PEDOT-20 and MnHCF@PEDOT-50 correspond to the formulas of $Na_{1.77}Mn[Fe(CN)_6]_{0.96}\square_{0.04}\cdot 1.75H_2O$, $Na_{1.71}Mn[Fe(CN)_6]_{0.94}\square_{0.06}\cdot 1.66H_2O$ and $Na_{1.56}Mn[Fe(CN)_6]_{0.90}\square_{0.10}\cdot 1.37H_2O$ with the mass fractions of the PEDOT coating layer 5.4 wt%, 12.4 wt% and 25.1 wt%, respectively. All the results clearly verify the Na-rich nature of these samples.

Raman spectra was carried out to verify the PEDOT coating as shown in **Fig. 1**b. In the bare MnHCF, there are two sharp peaks at 2079 and 2123 cm^{-1}, corresponding to the stretching vibrations of -C≡N-.[37] In the bare PEDOT, the stretching of the symmetrical C_α=C_β band is observed at 1438 cm^{-1}, and the peaks at 1502 and 1563 cm^{-1} are assigned to asymmetric C_α=C_β band stretching mode. Compared with the standard peaks, these main peaks of PEDOT in MnHCF@PEDOT composites shift upward, indicating that PEDOT is well oxidized.[35] The peak intensity of PEDOT increases while that of MnHCF decreases, and the relative intensity of the peak at 2123 cm^{-1} weakens, indicating an excellent composite and the decrease in the average valence state of transition metals in MnHCF.[37] In order to better understand the in-situ polymerization process, XPS was carried out as shown in **Fig. S2**. During the in-situ polymerization

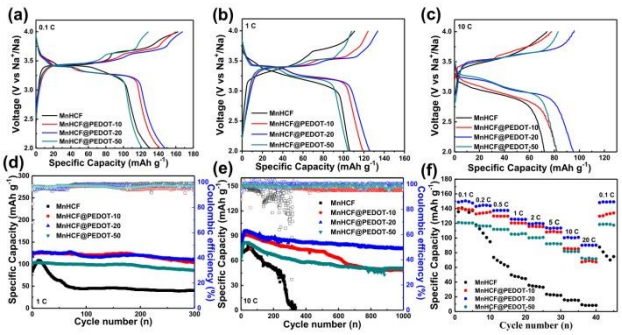

Fig. 2 Galvanostatic charge–discharge profiles at (a) 0.1 C, (b) 1 C and (c) 10 C cycled between 2.0 and 4.0 V; cycling performance and coulombic efficiency at (d) 1 C and (e) 10 C; (f) rate capability at various rates from 0.1 C to 20 C.

process, surface Fe^{3+} acts as an oxidant to induce EDOT to polymerize on the surface of MnHCF particles to PEDOT, while the valence of Mn remains unchanged. All these results clearly verify the tight binding between PEDOT and MnHCF, which is essential in improving the electronic conduction and enhancing the structure stability during cycling. Fig. 1c-h show the morphologies of bare MnHCF and MnHCF@PEDOT-20. The size of MnHCF particles varies from several hundred nanometers to several micrometers. Large particles have regular rectangular shape, while the shapes of most small particles are sphere-like, both of which exhibit smooth surface characteristics. Conversely, the surface of MnHCF@PEDOT-20 particles becomes rough due to the PEDOT coating, although the particle size doesn't change significantly. The above phenomenon is also verified through TEM, as shown in Fig. 1e and h. The edge of the MnHCF particles is smooth, while the edge of MnHCF@PEDOT-20 particles has a thin and rough PEDOT layer, manifesting the successful coating of PEDOT.

The galvanostatic charge-discharge profiles at 0.1 C (1 C = 150 mA g^{-1}) are shown in **Fig. 2**a. MnHCF displays two long voltage plateaus at ~3.4 V and ~3.7 V during charge, but only one voltage plateau at ~3.4 V during discharge. The charge and discharge capacities of MnHCF are 162.5 and 130.2 mAh g^{-1} respectively, manifesting the severe irreversibility during the initial charge/discharge process. For MnHCF@PEDOT, another voltage plateau at ~3.3 V is observed during discharge, possibly owing to the improved conductivity after PEDOT coating. With the increasing PEDOT mass fraction, charge/discharge capacities increase initially and then decrease, and MnHCF@PEDOT-20 shows the highest charge capacity of 167.7 mAh g^{-1} and the highest discharge capacity of 147.9 mAh g^{-1}, with a improved Coulombic efficiency (CE) of 88.2%. However, MnHCF@PEDOT-50 exhibits a lower capacity than MnHCF, since PEDOT has little Na storage activity (**Fig. S4**). As the current rate increases to 1 C (**Fig.2**b), the MnHCF suffers more severe polarization during cycling, accompanied with voltage plateaus changing into slopes. However, MnHCF@PEDOT still displays two distinct voltage plateaus during charge and discharge, and the polarization is much lower. Furthermore, MnHCF@PEDOT-20 delivers a highest charge capacity of 133.9 mAh g^{-1} and discharge capacity of 125.7 mAh g^{-1}, corresponding to a CE of 93.9%. When the current density reaches 10 C, specific capacities of all

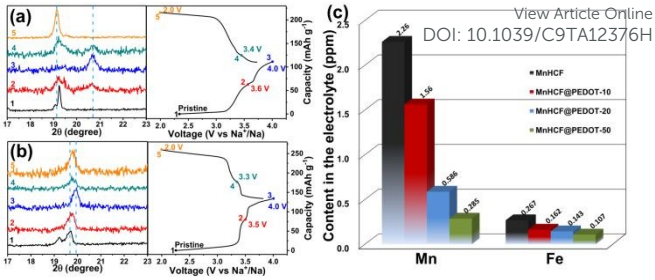

Fig. 3 Ex-situ XRD patterns of (a) MnHCF and (b) MnHCF@PEDOT-20; (c) contents of Mn/Fe in the electrolyte after 100 cycles.

MnHCF@PEDOT samples are much higher than bare MnHCF, as shown in **Fig. 2**c.

Fig. 2d compares the cycling performance of MnHCF and MnHCF@PEDOT at 1 C. The capacity of MnHCF increases continuously in the first ten cycles, indicating the existence of activation process, but the activation in MnHCF@PEDOT is inapparent. A highest discharge capacity of 106.0 mAh g^{-1} is observed at the 10th cycle for MnHCF and only a capacity of 44.3 mAh g^{-1} remains after 100 cycles. On the contrary, MnHCF@PEDOT-20 delivers the highest discharge capacity of 125.7 mAh g^{-1} at the 10th cycle, and remains 117.0 mAh g^{-1} (93.1%) after 100 cycles and 109.2 mAh g^{-1} (86.9%) even after 300 cycles, manifesting that PEDOT significantly improves the cycling stability of MnHCF. Cycling performances of all the MnHCF@PEDOT samples are also more outstanding than bare MnHCF at 10 C as shown in **Fig. 2**e. MnHCF@PEDOT-20 presents the highest discharge capacity of 95.2 mAh g^{-1} and remains 74.4 mAh g^{-1} (78.2%) after 1000 cycles. In contrast, the capacity of bare MnHCF decays rapidly to 0 after 330 cycles. Although MnHCF@PEDOT-10 has a capacity close to MnHCF@PEDOT-20, its capacity fading is worse and only remains 48.5 mAh g^{-1} (53.4%) after 1000 cycles, probably due to its imperfection of PEDOT coating layer.

Ex-situ XRD was applied to track the structural evolution upon Na^+ extraction and insertion of MnHCF and MnHCF@PEDOT-20. As shown in **Fig. 3**a and b, due to the cooperative Jahn-teller distortion of Mn^{3+} in MnN_6 octahedra, the MnHCF electrode experiences a two-phase transition between cubic and tetragonal during the cycle, while MnHCF@PEDOT-20 electrode maintains the monoclinic phase with a peak shift of only 0.27°, demonstrating the stability in structure during cycling. The PEDOT coating suppresses the phase transition during the cycle and reduces the volume change, thereby retarding the dissolution of electrode and improving the cycle stability of the electrode. On the other hand, it is known that in the presence of water, $NaPF_6$ salt is likely to decompose and generated hazardous substances such as HF, which accelerates the deterioration of the surface structure of MnHCF and leads to the dissolution of Mn/Fe, and ultimately leads to performance degradation during cycling. In order to determine the inhibition of the coating on the dissolution of Mn/Fe, ICP-OES was used to test the contents of Mn and Fe in the electrolyte after 100 cycles. An amplified half-cell was made as shown in **Fig. S5** to check the concentrations of transition metals in the electrolyte. After 100 cycles, the contents of Mn and Fe in the electrolyte of bare MnHCF are 2.26 and 0.267 mg L^{-1}, respectively, as shown in **Fig. 3**c. For

View Article Online
DOI: 10.1039/C9TA12376H

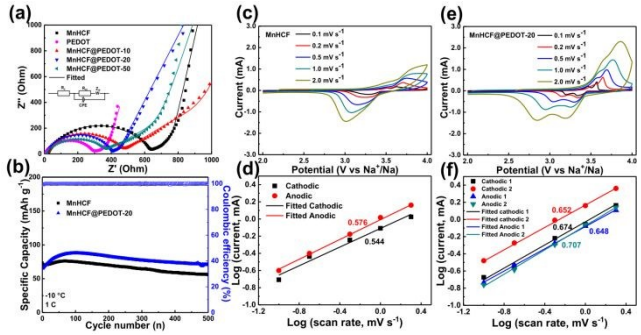

Fig. 4 (a) EIS spectra at the 10th cycle in a fully discharged state over the frequency range of 10^{-2}-10^{5} Hz; (b) Cycling performance and CE at -10 °C, 1 C; CV curves at scan rates ranging from 0.1 to 2.0 mV s^{-1} of (c) MnHCF and (e) MnHCF@PEDOT-20; the b-value calculation with the peak currents and the scan rates for (d) MnHCF and (f) MnHCF@PEDOT-20.

comparison, the contents of Mn and Fe in the electrolyte of MnHCF@PEDOT-20 are only 0.586 and 0.143 mg L^{-1}. It shows that the excellent cycling stability of MnHCF@PEDOT-20 can be attributed to the inhibition of side reactions and dissolution of transition metals, especially Mn, by PEDOT coating. In addition, as shown in **Fig. S6**, after 1000 cycles at 10 C or etching in 0.1 M HF solution at 100 °C for 4 h, the morphology of MnHCF@PEDOT-20 remains well, while MnHCF is destroyed, further indicating that the coating can well protect MnHCF from HF etching, and thus can inhibit the dissolution of Mn/Fe to maintain structural stability.

The rate capability of MnHCF and MnHCF@PEDOT are shown in **Fig. 2**f. As the current rate increases from 0.1 to 0.2, 0.5, 1, 2, 5, 10, and 20 C, the reversible specific capacity of MnHCF@PEDOT-20 slightly decreases from 148.8 to 142.9, 137.3, 125.6, 119.3, 113.8, 100.3, and 90.1 mAh g^{-1}, respectively. Moreover, the capacity recovers to 148.2 mAh g^{-1} when the current rate returns to 0.1 C. MnHCF@PEDOT-10 and MnHCF@PEDOT-50 also show good rate capability. On the contrary, the specific capacity of bare MnHCF decays rapidly with increasing current rate. Only a capacity of 8.4 mAh g^{-1} can be obtained at 20 C and the capacity is only 87.5 mAh g^{-1} when the current rate returns to 0.1 C. It can be observed that there's a significant improvement in rate performance of MnHCF, which might be ascribed to the promotion in electronic conduction of the electrode materials caused by tightly integrated PEDOT coating. Such electrochemical performance of our MnHCF@PEDOT-20 exceeds most state-of-the-art MnHCF electrodes for SIBs as summarized in **Table S1**. EIS tests of MnHCF and MnHCF@PEDOT electrodes were carried out to further elucidate the effect of PEDOT on the electrochemical properties of the electrodes. As shown in **Fig. 4**, an equivalent circuit is used to fit the Nyquist plot, the R_{ct} of MnHCF, MnHCF@PEDOT-10, MnHCF@PEDOT-20, MnHCF@PEDOT-50 and PEDOT are 602.9, 427.5, 373.8, 343.8 and 285.8 Ω, respectively. With the increase of PEDOT content, R_{ct} of MnHCF@PEDOT decreases due to promotion of the electronic conduction of the electrode, resulting in a boosted rate performance.

CV tests of bare MnHCF and MnHCF@PEDOT-20 at different sweep rates were conducted to further illuminate the electrochemical process of the electrodes. As shown in **Fig. S7**, MnHCF shows three cathodic peaks and two anodic peaks at a sweep rate of 0.1 mV s^{-1}, and the anodic peak at 3.55 V is very weak, while MnHCF@PEDOT-20 shows two pairs of sharp redox peaks, which correspond to the GCD results. The cathodic peak at 3.71 V and the small anodic peak at 3.55 V of MnHCF is supposed to be resulted from the polarization caused by the poor conductivity of MnCHF after partial Na extraction.[34, 38] As shown in **Fig. 4**c and e, with the increase of sweep rate, MnHCF exhibits only one pair of redox peaks, while MnHCF@PEDOT-20 still exhibits two pairs of redox peaks. The linear fitting results of log (peak current densities, i) and log (scanning rates, *v*) are shown in **Fig. 4**d and f according to the above CV curves. According to equation (1), *b* value can be obtained from the slope rate of the fitting line of log (i) vs. log (*v*).[39]

$$i = av^{b} \quad (1)$$

b = 0.5 indicates that the sodium storage mechanism is diffusion controlled. Conversely, *b* = 1.0 represents a capacitive process. For MnHCF, *b* values are 0.576 for the anodic peak and 0.554 for the cathodic peak, indicating that Na-diffusion kinetics is mainly diffusion controlled. However, for MnHCF@PEDOT-20, the *b* values of two anodic peaks are 0.648 and 0.707, and the *b* values of two cathodic peaks are 0.674 and 0.652, suggesting the enhancement of the capacitive process, which results in faster ion transfer and reaction kinetics of the MnHCF@PEDOT-20 electrode. When the temperature drops to -10 °C, the decomposition of $NaPF_6$ slows down, and the side reactions and dissolution of transition metals are weakened, resulting in good cycling stability and high CE of all electrodes as shown in Fig. 4b. However, since MnHCF@PEDOT is better in electronic conduction, the polarization is much decreased and hence MnHCF@PEDOT-20 exhibits higher capacity with 71.5 mAh g^{-1} (82.2 %), as compared to that of bare MnHCF with 55.9 mAh g^{-1} (73.36 %) after 500 cycles.

Conclusions

In summary, a series of MnHCF@PEDOT composites were successfully prepared through co-precipitation followed by a facile in-situ polymerization method. Such tightly binding PEDOT surface layer on MnHCF boosts the electronic conduction and capacitive storage, and on the other hand, effectively suppresses phase transition, inhibits the side reactions and the transition metal dissolution when used as cathodes for SIBs. The resultant MnHCF@PEDOT-20 composite exhibits excellent rate capability with a high capacity as high as 147.9 mAh g^{-1} at 0.1 C, 95.2 mAh g^{-1} at 10 C, and retains 90.2 mAh g^{-1} at 20 C, and a long cycle life with a retained capacity of 74.4 mAh g^{-1} (78.2%) at 10 C after 1000 cycle. Even at a low temperature of -10 °C, MnHCF@PEDOT-20 still delivers a high capacity of 87.0 mAh g^{-1} and retains 71.5 mAh g^{-1} (82.2 %) after 500 cycles. The present work offers a rational strategy in improving the electrochemical performance of PBAs for rechargeable batteries.

Conflicts of interest

The authors declare no competing financial interests.

Acknowledgements

This study was supported by National Natural Science Foundation of China (Grant No. 51722105), Zhejiang Provincial Natural Science Foundation of China (LR18B030001), and the Fundamental Research Funds for the Central Universities (2018XZZX002-08).

Notes and references

1 Z. Xing, S. Wang, A. Yu and Z. Chen, *Nano Energy*, 2018, **50**, 229-244.
2 H. Pan, Y.-S. Hu and L. Chen, *Energy & Environmental Science*, 2013, **6**, 2338.
3 N. Ortiz-Vitoriano, N. E. Drewett, E. Gonzalo and T. Rojo, *Energy & Environmental Science*, 2017, **10**, 1051-1074.
4 J. Y. Hwang, S. T. Myung and Y. K. Sun, *Chemical Society Reviews*, 2017, **46**, 3529-3614.
5 F. Xie, Z. Xu, A. C. S. Jensen, H. Au, Y. Lu, V. Araullo-Peters, A. J. Drew, Y. S. Hu and M. M. Titirici, *Advanced Functional Materials*, 2019, **29**, 1901072.
6 M. J. Piernas-Muñoz, E. Castillo-Martínez, J. L. Gómez-Cámer and T. Rojo, *Electrochimica Acta*, 2016, **200**, 123-130.
7 B. Wang, Y. Han, Y. Chen, Y. Xu, H. Pan, W. Sun, S. Liu, M. Yan and Y. Jiang, *Journal of Materials Chemistry A*, 2018, **6**, 8947-8954.
8 J. Song, B. Xiao, Y. Lin, K. Xu and X. Li, *Advanced Energy Materials*, 2018, **8**, 1703082.
9 W. Luo, Y. Zhang, S. Xu, J. Dai, E. Hitz, Y. Li, C. Yang, C. Chen, B. Liu and L. Hu, Nano Letter, 2017, 17, 3792-3797.
10 J. Conder and C. Villevieille, *Chemical Communications*, 2019, **55**, 1275-1278.
11 L. Fang, Z. Lan, W. Guan, P. Zhou, N. Bahalawane, W. Sun, Y. Lu, C. Liang, M. Yan, Y. Jiang, *Energy Storage Materials*, 2019, **18**, 107-113.
12 Y. Cao, L. Xiao, W. Wang, D. Choi, Z. Nie, J. Yu, L. V. Saraf, Z. Yang and J. Liu, *Advanced Materials*, 2011, **23**, 3155-3160.
13 H. Kim, R. A. Shakoor, C. Park, S. Y. Lim, J.-S. Kim, Y. N. Jo, W. Cho, K. Miyasaka, R. Kahraman, Y. Jung and J. W. Choi, *Advanced Functional Materials*, 2013, **23**, 1147-1155.
14 Y. Fang, L. Xiao, X. Ai, Y. Cao and H. Yang, *Advanced Materials*, 2015, **27**, 5895-5900.
15 H. Kim, I. Park, S. Lee, H. Kim, K.-Y. Park, Y.-U. Park, H. Kim, J. Kim, H.-D. Lim, W.-S. Yoon and K. Kang, *Chemistry of Materials*, 2013, **25**, 3614-3622.
16 Y. Jiang, S. Yu, B. Wang, Y. Li, W. Sun, Y. Lu, M. Yan, B. Song and S. Dou, *Advanced Functional Materials*, 2016, **26**, 5315-5321.
17 Y. You, H. R. Yao, S. Xin, Y. X. Yin, T. T. Zuo, C. P. Yang, Y. G. Guo, Y. Cui, L. J. Wan and J. B. Goodenough, *Advanced Materials*, 2016, **28**, 7243-7248.
18 Y. Qiao, G. Wei, J. Cui, M. Zhang, X. Cheng, D. He, S. Li and Y. Liu, *Chemical Communications*, 2019, **55**, 549-552.
19 B. Wang, Y. Han, X. Wang, N. Bahlawane, H. Pan, M. Yan and Y. Jiang, *IScience*, 2018, **3**, 110-133.
20 B. Wang, S. Liu, B. Pan, W. Sun, Y. Tang, H. Pan, M. Yan, Y. Jiang, *ChemSusChem*, 2019, **7**, 2415-2420.
21 L. Wang, J. Song, R. Qiao, L. A. Wray, M. A. Hossain, Y. D. Chuang, W. Yang, Y. Lu, D. Evans, J. J. Lee, S. Vail, X. Zhao, M. Nishijima, S. Kakimoto and J. B. Goodenough, *Journal of the American Chemical Society*, 2015, **137**, 2548-2554.
22 Y. Lu, L. Wang, J. Cheng and J. B. Goodenough, *Chemical Communications*, 2012, **48**, 6544-6546.
23 L. Wang, Y. Lu, J. Liu, M. Xu, J. Cheng, D. Zhang and J. B. Goodenough, *Angewandte Chemie*, 2013, **52**, 1964-1967.
24 P. Ge, S. Li, H. Shuai, W. Xu, Y. Tian, L. Yang, G. Zou, H. Hou and X. Ji, *Advanced Materials*, 2019, **31**, e1806092.
25 X. Bie, K. Kubota, T. Hosaka, K. Chihara and S. Komaba, *Journal of Power Sources*, 2018, **378**, 322-330.
26 X. Jiang, H. Liu, J. Song, C. Yin and H. Xu, *Journal of Materials Chemistry A*, 2016, **4**, 16205-16212.
27 H. Kim, G. Yoon, I. Park, K.-Y. Park, B. Lee, J. Kim, Y.-U. Park, S.-K. Jung, H.-D. Lim, D. Ahn, S. Lee and K. Kang, *Energy & Environmental Science*, 2015, **8**, 3325-3335.
28 C. Wang, L. Xing, J. Vatamanu, Z. Chen, G. Lan, W. Li and K. Xu, *Nature Communications*, 2019, **10**, 3423.
29 S. Zhang, H. Gu, H. Pan, S. Yang, W. Du, X. Li, M. Gao, Y. Liu, M. Zhu and L. Ouyang, *Advanced Energy Materials*, 2017, **7**, 1601066.
30 Y. Moritomo, S. Urase and T. Shibata, *Electrochimica Acta*, 2016, **210**, 963-969.
31 D. Yang, J. Xu, X. Z. Liao, Y. S. He, H. Liu and Z. F. Ma, *Chemical Communications*, 2014, **50**, 13377-13380.
32 J. Song, L. Wang, Y. Lu, J. Liu, B. Guo, P. Xiao, J. J. Lee, X. Q. Yang, G. Henkelman and J. B. Goodenough, *Journal of the American Chemical Society*, 2015, **137**, 2658-2664.
33 W. Li, S. Chou, J. Wang, J. Wang, Q. Gu, H. Liu and S. Dou, *Nano Energy*, 2015, **13**, 200-207.
34 Y. Mao, Y. Chen, J. Qin, C. Shi, E. Liu and N. Zhao, *Nano Energy*, 2019, **58**, 192-201.
35 S. Kulandaivalu, Z. Zainal and Y. Sulaiman, *International Journal of Polymer Science*, 2016, **2016**, 1-12.
36 S. Yu, Y. Li, Y. Lu, B. Xu, Q. Wang, M. Yan and Y. Jiang, *Journal of Power Sources*, 2015, **275**, 45-49.
37 Y. Tang, W. Zhang, L. Xue, X. Ding, T. Wang, X. Liu, J. Liu, X. Li and Y. Huang, *Journal of Materials Chemistry A*, 2016, **4**, 6036-6041.
38 Y. Liu, D. He, R. Han, G. Wei and Y. Qiao, *Chemical Communications*, 2017, **53**, 5569-5572.
39 Y. Jiang, Y. Li, P. Zhou, Z. Lan, Y. Lu, C. Wu and M. Yan, *Advanced Materials*, 2017, **29**.

View Article Online
DOI: 10.1039/C9TA12376H

A table of contents entry

In-situ polymerization is used to obtain PEDOT tightly coated MnHCF, inhibiting the phase transition and Mn dissolution during cycling.